ISSN 1070-3284, Russian Journal of Coordination Chemistry, 2020, Vol. 46, No. 9, pp. 653–661. © Pleiades Publishing, Ltd., 2020.

Two Heteroligand Cd(II)-Coordination Polymers: Crystal Structures and Anti-Lung Cancer Activity Evaluation

C. H. Ye[a], G. Chen[b], and Y. L. Gong[c, *]

[a] *Department of Oncology, Bazhong Central Hospital, Bazhong, Sichuan, P.R. China*

[b] *Department of Obstetrics and Gynecology, The Public Health Clinical Center of Chengdu, Chengdu, Sichuan, P.R. China*

[c] *Department of Neurology, Affiliated Sichuan Provincial Rehabilitation Hospital of Chengdu University of TCM, Chengdu, Sichuan, P.R. China*

*****e-mail: yulai_gong11@163.com*

Received October 16, 2019; revised November 6, 2019; accepted November 28, 2019

Abstract—Two new Cd(II) containing coordination polymers, namely $\{[Cd(Dib)(1,4\text{-}Ndc)] \cdot H_2O\}_n$ (**I**, Dib = 1,4-di(1*H*-imidazol-1-yl)butane, 1,4-H_2Ndc = naphthalene-1,4-dicarboxylic acid) and [Cd(2,2'-Dsb)-(Dpe)-(DMF)(H_2O)] (**II**, 2,2'-H_2Dsb = 2,2'-disulfanediyldibenzoic acid, Dpe = (*E*)-1,2-di(pyridin-4-yl)ethene), have been successfully prepared under the hydrothermal or solvothermal conditions by using the carboxylic acid and N-donor linkers with different functional groups as the co-ligands. Furthermore, the CCK-8 assay was performed to detect the inhibitory effect of these two synthetic complexes on the NCI-H292 lung cancer cell line. The mechanism of the complexes anti-cancer activity was explored with Annexin V-FITC/PI apoptosis detection and western blot assay.

Keywords: coordination polymers, mixed-ligand approach, diamond-like network, anti-cancer activity

DOI: 10.1134/S1070328420090080

INTRODUCTION

Structure and design of metal-involved coordination polymers composed of metal ion/clusters and organic ligands with the guide of crystal engineering are currently of interest in the field of supramolecular chemistry and coordination chemistry [1–3]. The increasing interest in this field is justified not only by their valuable unit structure, but also their potential applications in luminescence, catalysis and biochemistry particularly in modern medicinal chemistry [4–6]. Among the series of compounds fabricated, the functional complexes attract great attention due to the potential drug value applications [7–10]. Thus, selecting safe, efficient and biocompatible ligands has become a crucial factor in the field of structural design, drug therapy and clinical applications. Polydentate ligands such as polycarboxylic acids or nitrogen-containing heterocyclic ligands are widely used in the rational design and controlled synthesis of these multifunctional complexes. Recently, N-heterocyclic carboxylate ligands have attracted considerable attention of chemists and biologists because of their abundant coordination modes and functional properties, as well as hydrogen-bonding donors and acceptors under solution conditions. It is well known that carboxyl groups can possess potential coordination sites to adopt various coordination modes and the C=O groups can act as O-donors [11]. Furthermore, ligands containing N-donor and polycarboxylic moieties are often used for constructing coordination complexes because of their better binding ability with metal centers [12]. The recent literatures have revealed that some Cd(II)-based coordination complexes show promising anticancer activities. For instance, Karmakar and co-workers have found that the Cd-benzothiazole complexes are cytotoxic in pancreatic cancer cell lines Mia Paca-2, BxPC-3 and Panc-1 [13]. In this study, two new Cd(II) containing coordination polymers, namely $\{[Cd(Bib)(1,4\text{-}Tdc)] \cdot H_2O\}_n$ (**I**, Dib = 1,4-di(1H-imidazol-1-yl)butane and 1,4-H_2Ndc = naphthalene-1,4-dicarboxylic acid) and [Cd(2,2'-Dsb)(Dpe)(DMF)(H_2O)] (**II**, 2,2'-H_2Dsb = 2,2'-disulfanediyldibenzoic acid and Dpe = (E)-1,2-di(pyridin-4-yl)ethene), have been successfully prepared under the hydrothermal or solvothermal conditions by using the carboxylic acid and N-donor linkers with different functional groups as the co-ligands. The single crystal X-ray diffraction studies reveal that complex **I** is a 3D framework structure showing the 5-fold interpenetrating diamond-like network, while complex **II** shows a 3D supramolecular architecture formed by the stacking of the 1D chains via hydrogen bonding and C–H···π and π···π interactions. In the biological research, the anticancer activity of the two complexes has been studied via the CCK-8 assay on NCI-H292 lung cancer cell lines, the

results showed that complex **I** showed significantly stronger inhibitory effect on NCI-H292 lung cancer cell viability than complex **II**. And the apoptosis assay and western blot suggested that the anti-cancer activity of the complex on NCI-H292 cancer cells was due to the induction of NCI-H292 cancer cell apoptosis.

EXPERIMENTAL

Materials and instrumentation. All reagents and solvents were commercially available and used as received without further purification. The naphthalene-1,4-dicarboxylic acid and 2-mercaptobenzoic acid ligands were obtained from Shanghai Chemsoon Chemical Science and Technology Co., Ltd. (Shanghai, China). The N-donor ligands 1,4-di(1H-imidazol-1-yl)butane and (*E*)-1,2-di(pyridin-4-yl)ethane were purchased from Jinan Henghua Sci. & Tec. Co. Ltd. (Jinan, China). Elemental analyses for C, H and N were performed on a CHN-O-Rapid analyzer or an Elementar Vario MICRO analyzer. IR spectra were recorded with a Thermo Scientific Nicolet 5700 FT-IR spectrophotometer with KBr pellets from 400 to 4000 cm^{-1}. Powder X-ray diffraction (PXRD) data were collected on a Bruker D8 Advance instrument using CuK_α radiation (λ = 1.54056 Å) at room temperature. The thermogravimetric (TG) analysis was carried on a Netzsch STA 449C thermal analyzer at a heating rate of 10°C min^{-1} in a N_2 atmosphere.

Synthesis of complexes I and II. For complex **I**, a mixture of $Cd(OAc)_2 \cdot 2H_2O$ (0.0532 g, 0.2 mmol), 1,4-H_2Ndc (0.0432 g, 0.2 mmol), Dib (0.0380 g, 0.2 mmol) and H_2O (10 mL) was adjusted to pH 7 with HNO_3 (1 M), stirred for 0.5 h, and then transferred and sealed in 25 mL Teflon-lined stainless steel container, which was heated at 120°C for 48 h and then cooled to room temperature at a rate of 10°C h^{-1}. After cooling to room temperature, light yellow block crystals of **I** were obtained (the yield was 77%).

For $C_{22}H_{22}N_4O_5Cd$

Anal. calcd., %	C, 49.40	H, 4.15	N, 10.48
Found, %	C, 49.62	H, 4.13	N, 10.72

Complex **II** was synthesized via in situ ligand synthesis. A solution of Dpe (0.036 g, 0.2 mmol) in MeOH (2 mL) was added into a solution of $Cd(NO_3)_2 \cdot 4H_2O$ (0.062 g, 0.2 mmol) in DMF (2 mL) followed by the addition of 2-mercaptobenzoic acid (0.031 g, 0.2 mmol). The mixture was then transferred and sealed in 25 mL Teflon-lined stainless steel container, which was heated at 100°C for 48 h and then cooled to room temperature at a rate of 10°C h^{-1}. After cooling to room temperature, the yellow color block crystals of **II** were obtained (0.10 g, the yield was 70% based on Cd). Under the experimental conditions employed, an oxidative medium is favoured and leads to the formation of the S–S bond.

For $C_{29}H_{27}N_3O_6S_2Cd$

Anal. calcd., %	C, 49.40	H, 4.15	N, 10.48
Found, %	C, 49.29	H, 4.02	N, 10.26

X-ray crystal structure determination. The structure data of complexes **I**, **II** were collected on a Super Nova diffractometer equipped with a CuK_α (λ = 1.5406 Å) and an Atlas CCD detector. These structures were resolved by direct methods and refined by full-matrix least squares fitting on F^2 using the SHELX-2016 software package [14]. All non-hydrogen atoms were refined with anisotropic thermal parameters except the solvent molecules. The hydrogen atoms on the aromatic rings were located at geometrically calculated positions and refined by riding. A summary of crystallographic parameters and refinement results are listed in Table 1.

Cell counting kit-8 assay (CCK-8). Stock solutions of grinded complexes **I** and **II** were prepared in DMSO (Sigma Aldrich) at a concentration of 1000 μM, which were sterilized by filtration through Millipore filter (0.22 μM) before use, and diluted by cell culture medium to various working concentrations. CCK-8 was performed according to the manufactures instructions in this experiment to detect the cell viability of NCI-H292 lung cancer cells and normal human lung cells BEAS-2B after incubated with complexes **I** and **II**. Briefly, NCI-H292 cells and normal human lung cells BEAS-2B in the logarithmic growth phase were collected and seeded onto 96-well plates with the final density of 1×10^3 cells per well, and then the plates were placed in an incubator of 37°C, 5% CO_2 humidified atmosphere for 12 h incubation. The complexes **I** and **II** (1, 2, 4, 8, 10, 20, 40, 80 μg/mL) were added into wells for 24 h incubation when the cells reached a 70–80% confluence, the ligands L^1 and H_2L^2 was added as the negative control. After complexes treatment, the cell medium was discarded and 100 μL CCK-8 solution was added for further incubation. Finally, the optical density values of each well were measured at 490 nm with a microplate reader (Bio-Rad, Hercules, CA). Cell viability (%) and IC_{50} was calculated according to the CCK-8 results. This experiment was repeated at least three times.

Annexin V-FITC/PI assay. After treated NCI-H292 lung cancer cells with the complexes **I** and **II**, as well as the ligands L^1 and H_2L^2 negative control, the detail mechanism was explored with the Annexin V-FITC/PI apoptosis kit (BD Biosciences, San Jose, CA, USA), and the cell apoptosis in NCI-H292 cells was measured in flow cytometer according to the protocols. In brief, NCI-H292 cells in the logarithmic growth phase were harvested and plated onto 6-well plates (2×10^5 cells per well), then the cells were cul-

Table 1. The crystallographic data and structure refinement for **I** and **II**

Parameter	Value	
	I	**II**
Empirical formula	$C_{22}H_{20}N_4O_4Cd$	$C_{29}H_{27}N_3O_6S_2Cd$
Formula weight	516.82	690.05
Temperature, K	296.15	296.15
Crystal system	Triclinic	Monoclinic
Space group	$P\bar{1}$	$P2_1/n$
a, Å	9.436(2)	7.7317(3)
b, Å	11.113(7)	17.7115(8)
c, Å	13.845(10)	23.3846(10)
α, deg	102.940(14)	90
β, deg	103.921(10)	99.182(2)
γ, deg	106.845(12)	90
Volume, Å^3	1279.6(12)	3161.3(2)
Z	2	4
ρ_{calcd}, g/cm^3	1.341	1.450
μ, mm^{-1}	0.884	0.867
Reflections total/unique	7288/5200	47174/6021
R_{int}	0.0525	0.0335
Reflections ($I \geq 2\sigma(I)$)	3050	5517
Data/restraints/parameter	5200/62/299	6201/36/373
Goodness-of-fit on F^2	0.936	1.084
Final R indexes ($I \geq 2\sigma(I)$)	$R_1 = 0.0623$, $wR_2 = 0.1096$	$R_1 = 0.0400$, $wR_2 = 0.1028$
Final R indexes (all data)	$R_1 = 0.1130$, $wR_2 = 0.1278$	$R_1 = 0.0460$, $wR_2 = 0.1064$
Largest diff. peak/hole, e Å^{-3}	0.51/−0.69	0.72/−1.25

tured in an incubator at 37°C, 5% CO_2 humidified condition overnight. When the cells reached a 70–80% confluence, serious dilutions of complexes **I** and **II** was added into wells for cell treatment. After complexes **I** and **II** treatment, the NCI-H292 cancer cells were washed, harvested and labeled with 5 μL Annexin V-FITC and 5 μL propidium iodide (PI) for 30 min in the dark. Finally, all the samples were detected by flow cytometry (BD, NJ, USA), and the results were analyzed using flow cytometry (FACS-Calibur, BD Biosciences, USA). All experiments were repeated three times.

Western blot assay. To detect the activation of the PTEN-AKT signaling pathway, the relative expression level of the PTEN and AKT protein was measured with the western blot assay in this study. After treated with indicated concentration of complexes **I** and **II**, was well as the ligands L^1 and H_2L^2 negative control, the total protein in NCI-H292 cancer cells were extracted using total Protein Extraction Kit (Invent Biotechnologies, under the guidance of the manufacturer's instructions). The BCA Protein Assay Kit (Beyotime Biotechnology) was used to measure the concentration of all samples, then the samples were added with 5× loading buffer for protein denaturation. The equal amount of protein samples was separated in 12% sodium dodecyl sulfate polyacrylamide gel, and then transferred onto 0.22 mm polyvinylidene fluoride (PVDF) membrane (Millipore, Bedford, MA, USA). After blocked with 5% BSA for one hour, the membranes were incubated with appropriate primary antibody at 4°C for 12 h. After that, the appropriate secondary horseradish peroxidase (HRP)-conjugated secondary antibodies (Jackson Immuno Research, West Grove, PA) were used to incubate with membranes for 1 h. Images were captured using Millipore Immobilon ECL illuminating solution (Millipore Corporation, USA).

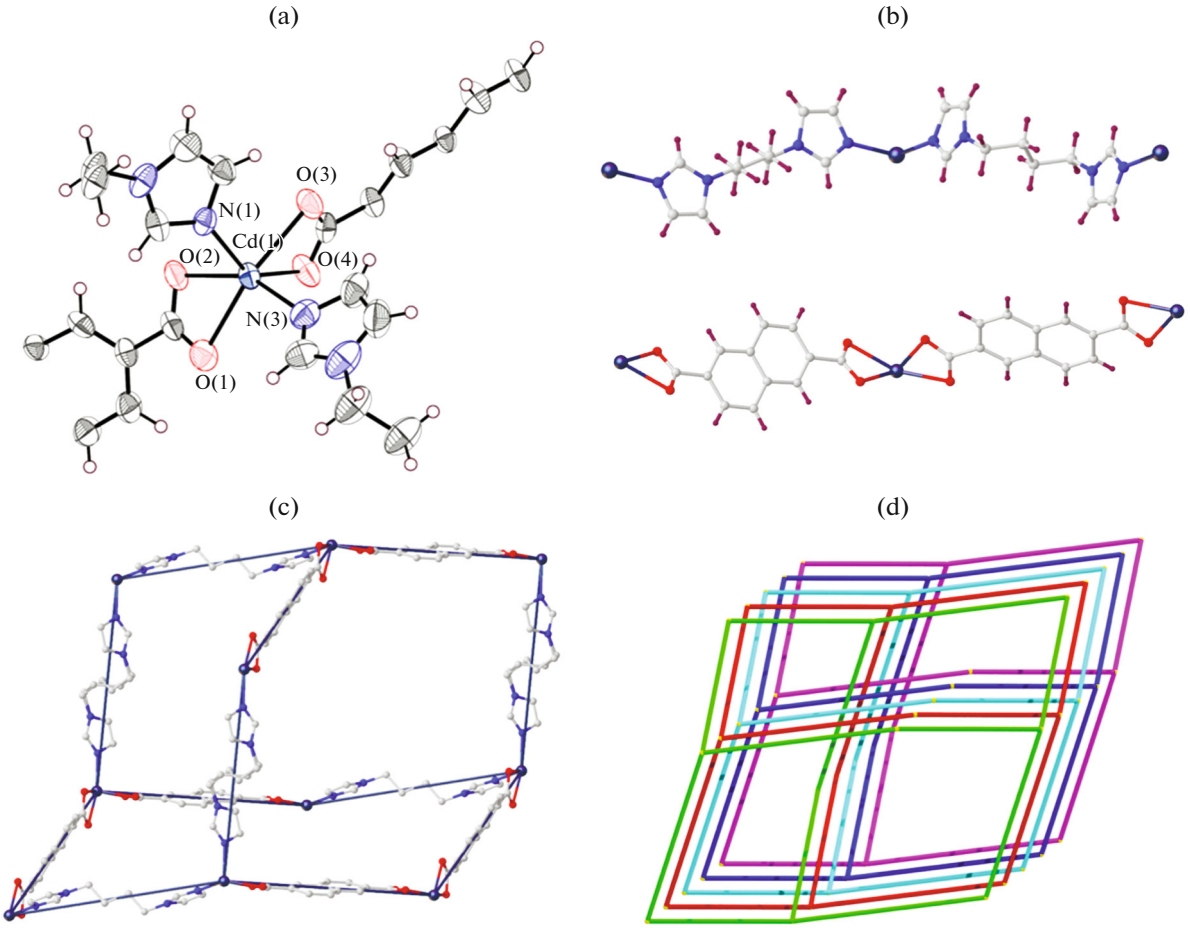

Fig. 1. View for the asymmetric unit of **I** (a), the coordination patterns for the two organic ligands (b), a single diamond-like cage of **I** (c), the 5-fold interpenetrating dia network viewed along the [100] direction (d).

RESULTS AND DISCUSSION

The complex **I** was prepared via a hydrothermal reaction of $Cd(OAc)_2 \cdot 2H_2O$ with the 1,4-H_2Ndc and the Dib ligand at pH value of 7 by using the HNO_3 as the pH modulator. The structural solution and refinement results based on the crystal data collected at room temperature shows that complex **I** crystallizes in the triclinic space group $P\bar{1}$ and reflected a 3D framework structure based on the six-coordinated Cd^{2+} ions as nodes. The asymmetric unit is composed of one Cd^{2+} ion, one Dib ligand, one 2,6-Ndc^{2-} ligand and one lattice water molecule. As depicted in Fig. 1a, Cd(II) ion is coordinated by two nitrogen atoms from two Dib ligands (Cd–N 2.236(5)–2.249(6) Å), and four carboxylic oxygen atoms from two 2,6-Ndc^{2-} ligands (CdO 2.323(4)–2.371(4) Å). Therefore, the coordination geometry of Cd^{2+} ion can be regarded as an elongated octahedron with N_2O_4 coordination node in which the equatorial plane is composed of four carboxylic oxygen atoms and two apical positions are occupied by two imidazole nitrogen atoms. Each 2,6-Ndc^{2-} acts as a linear building block linking two Cd^{2+} ions through two carboxyl groups which adopt the same μ_1-η^1:η^1 coordination mode. Each Dib ligand adopts a *trans*-conformation to bridge the Cd^{2+} ions into 1D chains (Fig. 1b). The extension of the structure of **I** into a 3D diamond network is accomplished by binding two Dib and 2,6-Ndc^{2-} ligands to the four-connected Cd(II) nodes. A single diamond-like framework is illustrated in Fig. 1c, which possesses maximum dimensions (the longest intracage distances between Cd···Cd) of 27.754 × 23.712 × 21.859 $Å^3$ (2a × 2b × 2c). Using a topological approach to gain a better insight into this framework, complex **I** can be described as dia net with the short and long symbols of 6^6 and ($6^2 \cdot 6^2 \cdot 6^2 \cdot 6^2 \cdot 6^2 \cdot 6^2$), respectively. The cavity is large enough to be filled via mutual entanglement of four independent equivalent frameworks, assembling a 5-fold interpenetrating dia net (Fig. 1d).

Single crystal X-ray crystallography revealed that complex **II** crystallizes in the monoclinic space group $P2_1/n$ with $Z = 4$, and reflects a 1D chain-like network based on the six-coordinated Cd^{2+} ions as nodes. The

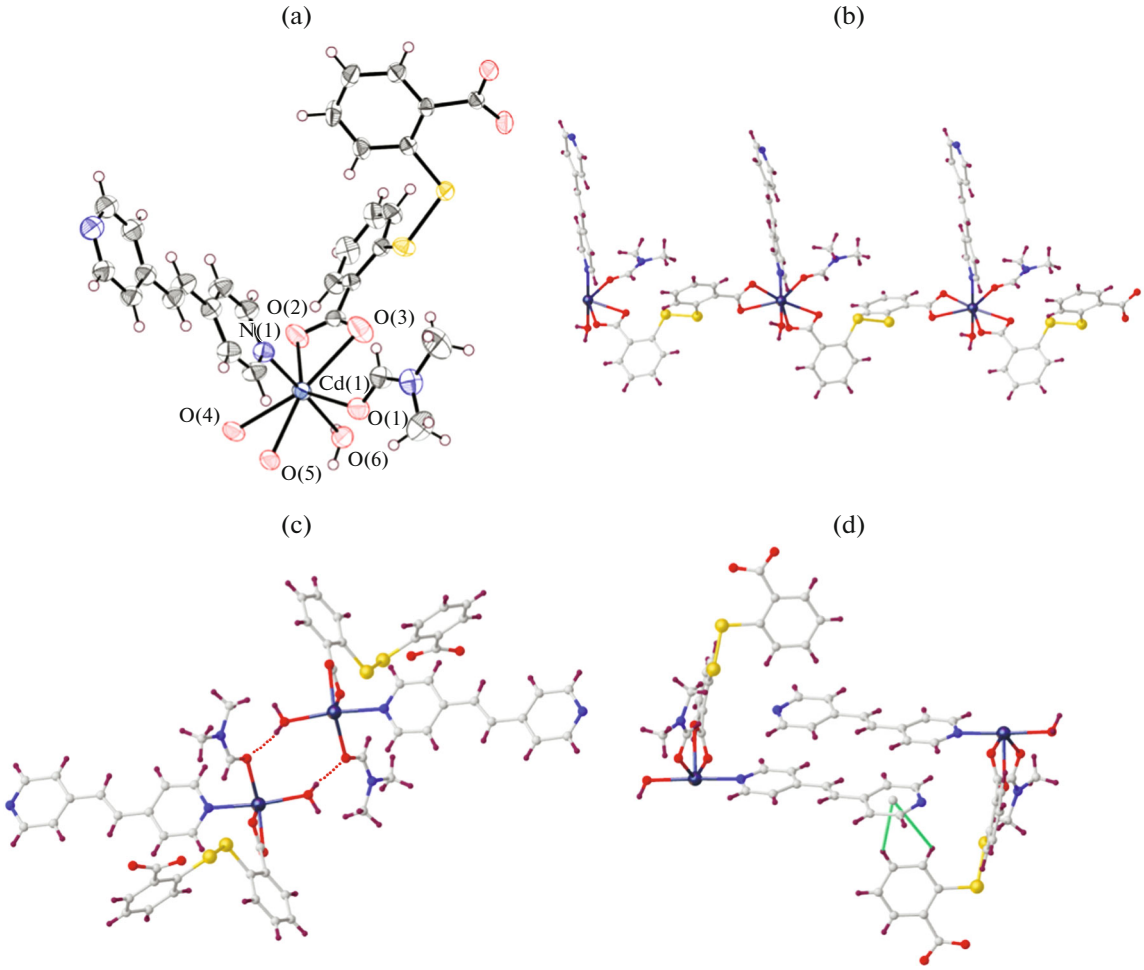

Fig. 2. Coordination environment of Cd^{2+} ions in **II** (a), the 1D chain-like structure in **II** (b), view for the H-bond (c) and C–H···π interactions in **II** (d).

asymmetric unit of **II** is composed of one crystallographically independent Cd^{2+} ion, one fully deprotonated 2,2'-Dsb ligand, one coordinated DMF and one coordinated water molecule. Each Cd(II) centre in **II** adopts a distorted pentagonal bipyramidal geometry and is ligated by five O atoms from two chelating 2,2'-Dsb anions (Cd–O 2.261(2)–2.528(2) Å) and one DMF ligand (Cd–O 2.385(2) Å) in the equatorial plane and by an O atom from an aqua ligand (Cd–O 2.314(2) Å) and one N atom from a Dpe ligand (Cd–N 2.293(2) Å) at the axial positions (Fig. 2a). The connectivity of carboxylate ligands with Cd(II) centers results in a 1D zigzag chain polymer (Fig. 2b). Here, the monomeric ligand 2,2'-Dsb gets dimerized via S–S bond formation, which leads to the formation of the 1D chain. The S–S bond length is 2.046(1) Å, which is comparable to the reported distances in the literature [15–17]. Here, due to the S–S bond formation, the structure becomes flexible and adopts a 1D zigzag chain structure. In addition, there is a strong intramolecular sulphur–oxygen interaction (S···O 0.751 Å) present in the 2,2'-Dsb ligand which results in the roughly sinusoidal S···O bonded chains. The 1D chains further undergo intermolecular hydrogen bonding interactions between the aqua ligand and O atoms of the 2,2'-Dsb ligand with the O···O separation of 2.726–2.885 Å in the *bc* plane (Fig. 2c). Besides, there are extensive C–H···π interactions with edge-to-face distances of 2.755–2.853 Å (Fig. 2d). In the solid state structure, the cooperative hydrogen bonding along with C–H···π and H-bond interactions form a 3D supramolecular architecture.

In order to check the phase purity of complexes **I** and **II**, PXRD were recorded at room temperature (Fig. 3a). The results showed that the measured PXRD patterns correspond to the simulated patterns generated from the single crystal diffraction data, which indicates the phase purity of the synthesized samples. In view of the following bioactivity study, the stability of complexes **I** and **II** in the biological medium should be considered. To check the framework stability of complexes **I** and **II**, the freshly as-prepared samples were soaked in the biological medium

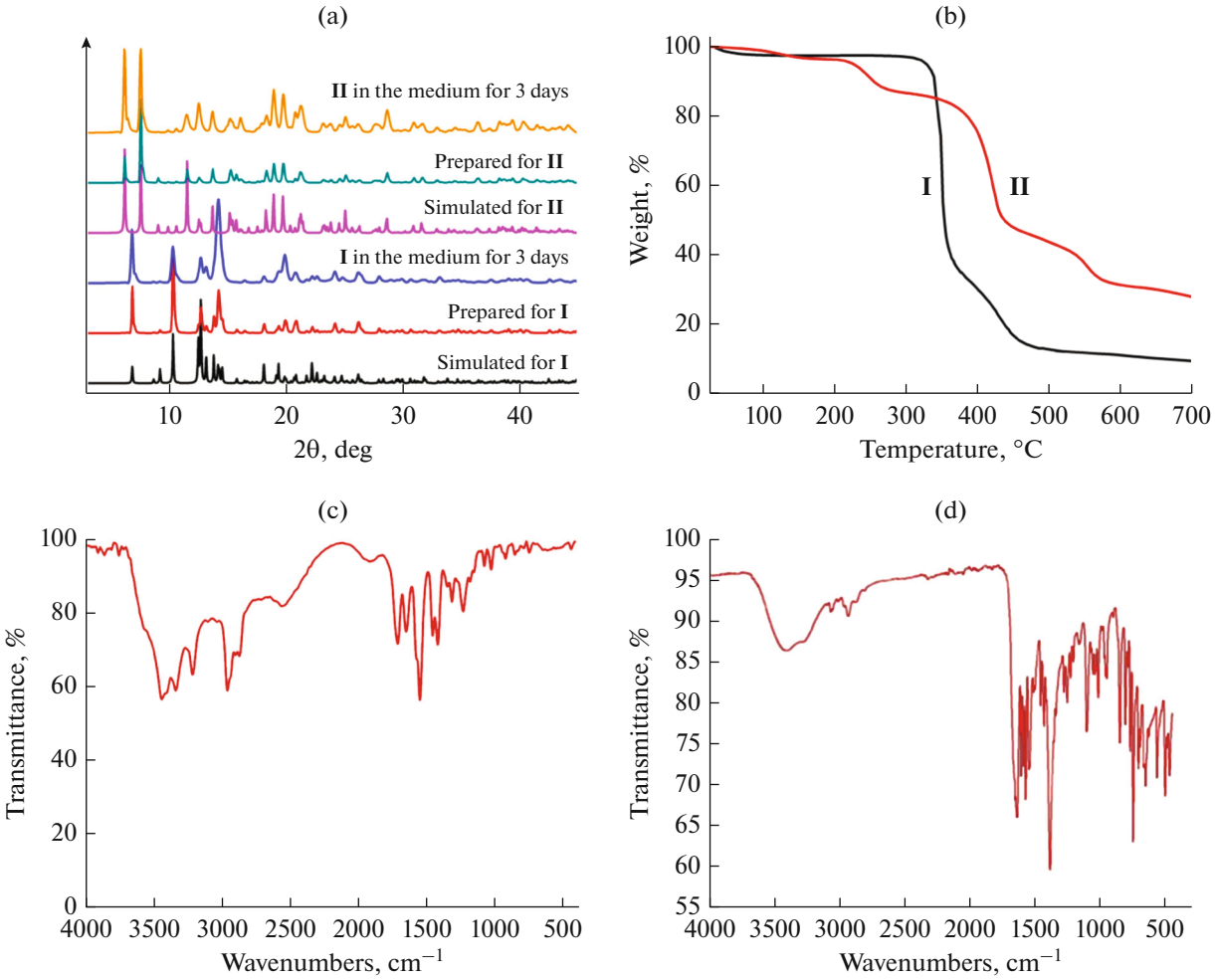

Fig. 3. The PXRD patterns of **I** and **II** (a), the TG curves for **I** and **II** (b), the FT-IR data for complexes **I** (c) and **II** (d).

for three days and then their corresponding PXRD patterns were collected, which reflect that the PXRD patterns of the treated samples are comparable with those of the as-prepared ones, indicating their good framework stability in the biological medium.

To check the thermal stability of **I** and **II**, the TG analysis was carried out under a linear heating rate of 5°C min^{-1} with a nitrogen atmosphere (Fig. 3b). For complex **I**, the TG curve reveals that it undergoes two weight-loss stages. The first stage starts at 35°C and ends at 88°C, accompanied by about 1.81% weight loss, which is attributed to the loss of one free water molecules (calcd. 1.62%). The second stage is observed from 325 to 375°C, considered as the collapse of the main framework and corresponding to the decomposition of the organic ligands. For complex **II**, the weight loss occurred in two stages corresponding to a loss of a coordinated water molecule and coordinated DMF. The total loss of 12.3% corresponds to the loss of water and DMF molecules (calcd. 13.0%). The complete decomposition of the complex occurs above 250°C. The IR spectra of the complexes **I** and **II** are presented in the Fig. 3c and Fig. 3d. The broad peaks around 3400 cm^{-1} in the IR spectra of the complexes **I** and **II** are mainly assigned to the ν(OH) stretching vibrations of hydrogen bonded water molecules. The absence of strong absorption bands in the 1700 cm^{-1} region confirms the fully deprotonation of the carboxylate groups in the ligand. The infrared bands 2950, 2890, and 2850 cm^{-1} in the complex **I** are associated with the CH_2 modes of the Dib ligand [18]. The bands around 1540 cm^{-1} and the bands between 1450 and 1410 cm^{-1} in complexes **I** and **II** are ascribed to ν_{asym} and ν_{sym} of the deprotonated carboxylate anions, respectively, $\Delta(\nu_{asym} - \nu_{sym}) < 200$ cm^{-1}, which indicates the deprotonated carboxyl groups of the 1,4-H_2Ndc and 2,2'-H_2Dsb ligands in the two coordination polymers coordinate to metal atoms in bidentate mode [19]. In addition, the peak at 471 cm^{-1} in complex **II** suggested the formation of the S–S bond [20]).

After the synthesis of the complexes **I** and **II**, their inhibitory effect on the viability of NCI-H292 lung cancer cells was evaluated in vitro. Firstly, the CCK-8

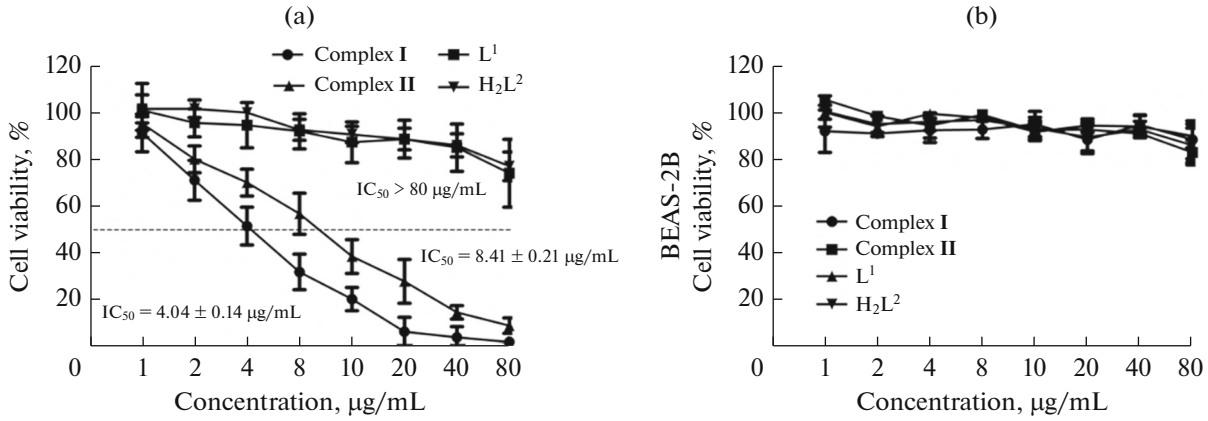

Fig. 4. Significantly reduced viability of NCI-H292 lung cancer cells and normal human lung cells BEAS-2B after complex **I** treatment. The NCI-H292 cells (a) and BEAS-2B cells (b) were exposed to different concentrations of complexes **I**, **II** and the related ligands, the cancer cell viability was measured by CCK-8 assay, and the IC_{50} was calculated. All experiments were performed in triplicate.

assay was performed to detect the effects of complexes **I** and **II** on NCI-H292 cancer cells in this experiment. After exposed to serious dilutions of complexes **I** and **II**, was well as the ligands L^1 and H_2L^2, the cell viability of NCI-H292 cancer cells was measured in a microplate reader. As the results showed in Fig. 4a, after treated with complex **I**, the viability of NCI-H292 cancer cells reduced remarkably in a dose-dependent manner with the IC_{50} of 4.04 ± 0.14 μg/mL. Complex **II**, ligands L^1 and H_2L^2 showed slightly influence on NCI-H292 cancer cells viability. While, Fig. 4b showed that complexes **I** and **II**, as well as ligands L^1 and H_2L^2 all showed no inhibitory effect on the viability of normal human lung cells BEAS-2B. These results indicated complex **I** has excellent anti-cancer activity on NCI-H292 cancer cells compared with complex **II** and the ligands, and all the complexes have no toxicity on normal human lung cells.

In the experiment above, we have confirmed that complex **I** showed excellent inhibitory on the NCI-H292 cancer cells viability in vitro. However, the detail mechanism this phenomenon was still unclear. Thus, in this experiment, Annexin V-FITC/PI apoptosis kit was used combined with flow cytometry to detect whether the complex exert the anti-cancer activity via inducing the cancer cell apoptosis. As results shown in Fig. 5, the percentage of apoptotic cells was increased to 73.59% under the treatment of complex **I**, which is significantly higher than that of complex **II** treatment (0.51%), as well as the ligands L^1 and H_2L^2. This data indicated that complex **I** has a stronger ability in inducing apoptosis in NCI-H292 cancer cells than complex **II**.

It is reported that the PTEN-AKT signal pathway plays an important role in cancer cell proliferation and apoptosis. Therefore, in this experiment, we aimed to explore whether the PTEN-AKT activation is influenced under complexes **I**, **II** and ligands L^1 and H_2L^2 treatment. As results shown in Fig. 6, after treated with complex **I**, the PTEN relative expression was increased significantly compared with control group. Consistently, the p-AKT, a common downstream target of PTEN, negatively regulated by PTEN, decreased remarkably. However, complex **II** and ligands L^1 or H_2L^2 has no effect on the activation level of PTEN-AKT signal pathway. This result indicated complex **I** has stronger induction effect on the PTEN-AKT signal pathway activation.

In summary, two new Cd(II) containing coordination polymers have been successfully prepared under the solvothermal conditions by using the different mixed-ligand systems. The as-prepared two coordination polymers have been characterized using the elemental analysis along with the single crystal X-ray analyses. The single crystal X-ray diffraction studies reveal that complex **I** is a 3D framework structure showing the 5-fold interpenetrating diamond-like network, while complex **II** shows a 3D supramolecular architecture formed by the stacking of the 1D chains via hydrogen bonding and C–H···π and π···π interactions. More importantly, we explored the anti-cancer activity of complexes **I**, **II**, as well as ligands L^1 and H_2L_2 on NCI-H292 lung cancer cells with CCK-8 assay, and the results indicated that complex **I** showed significantly stronger activity than complex **II** and the ligands. The apoptosis results suggested complex **I** could induce the apoptosis in NCI-H292 cells, and this induction ability was stronger than complex **II** or related ligands. As a critical pathway in cancer cell proliferation and apoptosis, the activation level of PTEN-AKT signaling was detected by western blot, we found complex **I** remarkably increased the expression of PTEN and reduced the level of p-AKT, but not complex **II** and the ligands. In conclusion, complex **I**

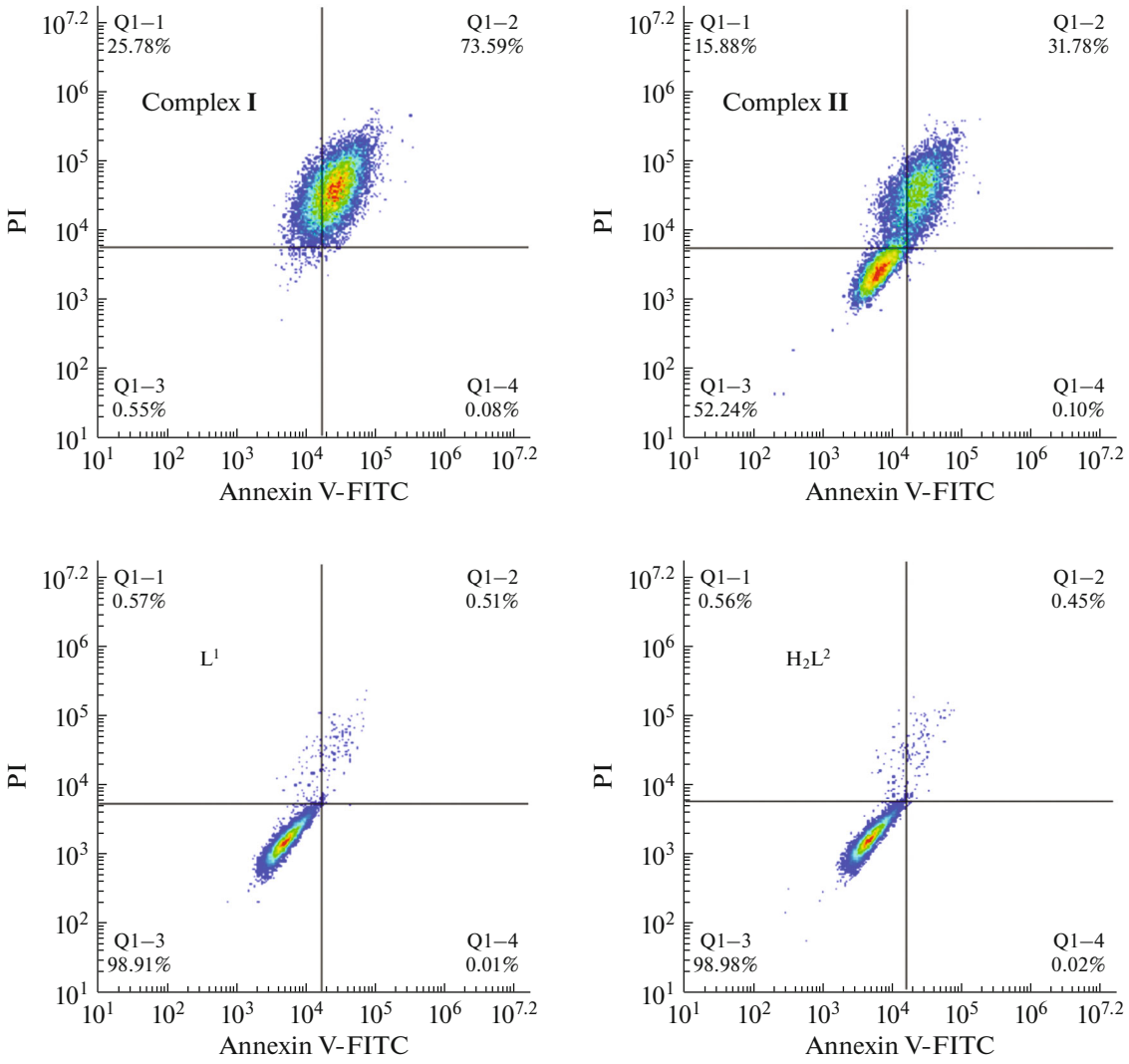

Fig. 5. Increased NCI-H292 lung cancer cells apoptosis induced by complexes **I** and **II** treatment. NCI-H292 cancer cells were treated with indicated concentration of complexes **I**, **II** and ligands L^1 and H_2L^2 for 24 h, then the cells were stained with Annexin V-FITC/PI solution and the apoptotic cells percentages were analyzed by flow cytometry. The experiment was repeated at least three times.

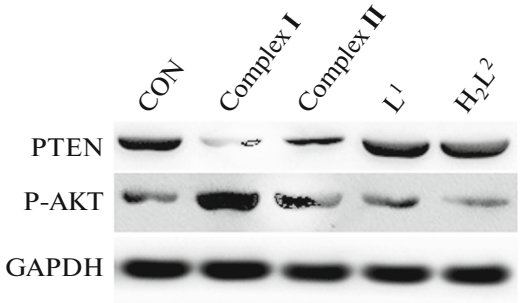

Fig. 6. Increased activation level of PTEN-AKT signaling in NCI-H292 lung cancer cells after complex treatment. NCI-H292 cancer cells were treated with indicated concentration of complexes **I**, **II** and ligands L^1 and H_2L^2 for 24 h. Western blot analysis was performed to detect the level of PTEN and p-AKT in NCI-H292 cancer cells.

is a potential anti-cancer candidate for further anti-cancer treatment.

REFERENCES

1. Wu, B., Zhang, W.H., Ren, Z.G., et al., *Chem. Commun.*, 2015, vol. 51, p. 14893.
2. Liu, B., Wei, L., Li, N.N., et al., *Cryst. Growth Des.*, 2014, vol. 14, p. 1110.
3. Han, Y., Sheng, S., Yang, F., et al., *J. Mater. Chem., A*, 2015, vol. 3, p. 12804.
4. Spokoyny, A.M., Kim, D., Sumrein, A., et al., *Chem. Soc. Rev.*, 2009, vol. 38, p. 1218.
5. Haldar, R., Matsuda, R., Kitagawa, S., et al., *Angew. Chem. Int. Ed.*, 2014, vol. 53, p. 11772.
6. Seco, J.M., Oyarzabal, I., Perez-Yanez, S., et al., *Inorg. Chem.*, 2016, vol. 55, p. 11230.

7. Raja, D.S., Bhuvanesh, N.S.P., and Natarajan, K., *Dalton Trans.*, 2012, vol. 41, p. 4365.
8. Wang, K., Ma, X., Shao, D., et al., *Cryst. Growth Des.*, 2012, vol. 12, p. 3786.
9. Wang, R.S., Feng, J., Lei, Y.Z., et al., *Cryst. Res. Technol.*, 2018, vol. 53, p. 1800065.
10. Zhang, N., Fan, Y., Zhang, Z., et al., *Inorg. Chem.* Commun., 2012, vol. 22, p. 68.
11. Mukherjee, S., Ganguly, S., Manna, K., et al., *Inorg. Chem.*, 2018, vol. 57, p. 4050.
12. Gao, E., Xing, J., Qu, Y., et al., *Appl. Organomet. Chem.*, 2018, vol. 32, p. e4469.
13. Karmakar, T., Kuang, Y., Neamati, N., et al., *Polyhedron*, 2013, vol. 54, p. 285.
14. Sheldrick, G.M., *Acta Crystallogr., Sect. C: Struct. Chem.*, 2015, vol. 71, p. 3.
15. Dutta, B., Jana, R., Sinha, C., et al., *Inorg. Chem. Front.*, 2018, vol. 5, p. 1998.
16. Feng, R., Jiang, F.L., Chen, L., et al., *Chem. Commun.*, 2009, vol. 49, p. 5296.
17. Liu, C.S., Yang, X.G., Hu, M., et al., *Chem. Commun.*, 2012, vol. 48, p. 7459.
18. Zhu, H., Liu, D., Li, Y.H., et al., *Inorg. Chem. Commun.*, 2019, vol. 108, p. 107539.
19. Zhao, X.X., Liu, D., Li, Y.H., et al., *Polyhedron*, 2018, vol. 156, p. 80.
20. Yu, X., Xie, J., Li, Y., et al., *J. Power Sources*, 2005, vol. 146, p. 335.